Journal of Environmental Chemical Engineering 10 (2022) 108258

Contents lists available at ScienceDirect

Journal of Environmental Chemical Engineering

journal homepage: www.elsevier.com/locate/jece

Green development of iron doped silica gel materials for chromium decontamination

David Gómez-Carnota, José L. Barriada *, Roberto Herrero

Universidade da Coruña, Departamento de Química & Centro de Investigaciones Científicas Avanzadas (CICA), 15071, A Coruña, Spain

ARTICLE INFO

Editor: Despo Kassinos

Keywords:
Chromium elimination
Polymerised silica gel
Iron dopped material

ABSTRACT

New hybrid polymeric materials were prepared by the polymerisation of sodium silicate, water, and hydrochloric acid, with the subsequent addition of iron. After the treatment with a natural reducing biomass extract, the resulting material was used in Cr(VI) decontamination processes. The preparation of the materials started with the synthesis of the polymeric base, and the successive modifications were made to maximise Cr(VI) removal. Characterization studies were carried out by SEM and EDS tests for each of the synthesised materials. The synthesised polymeric base (called GSP) was found to have a high affinity for Fe(II). An adsorption of 24.5 mg Fe (II)·g^{-1} on GSP was achieved, with an associated adsorption energy of 34.5 kJ·mol^{-1}. In the decontamination studies, the polymeric base acts as a Supporting material for iron, while the main Cr(VI) scavenger is the adsorbed Fe. Chromium removal takes place by a combined process of Cr(VI) reduction to Cr(III) and adsorption of both chromium species at acidic pH. An adsorption model, based on statistical thermodynamics, and removal rates were used to study the process. The proposed material is sustainable, cheap and has high capacity to remove chromium from aqueous media quickly and effectively.

1. Introduction

Environmental issues caused the human activity since last century are one of the most important challenges for science nowadays. Industry production is increasing every day due to our present lifestyle and needs and associated to this production, waste generation is also increasing. New efficient treatments must be developed to solve this problem and move towards more sustainable processes. A possible strategy is the development of new competitive materials which combine several elimination mechanisms to remove different types of pollutants, like organic compounds or metallic ions.

Among metals, a major concern about chromium (Cr) contamination is increasing worldwide because of the high concentration levels found in soil and water resulting from human activities. Chromium is considered the 17th (5th among metals) of 275 priority substance with most significant potential threat to human health by the Agency for Toxic Substances and Disease Registry (ATSDR) [1] and hazardous air pollutants (HAPs) and urban air toxicants by United States Environmental Protection Agency (US EPA) [2,3].

Chromium main oxidation states are Cr(VI) and Cr(III) in the range Eh-pH of natural waters. At low Eh environments, Cr(III) and its hydroxides are the main species [4]. On the contrary, Cr(VI) exists in solutions as ($HCrO_4^-$), (CrO_4^{2-}), ($Cr_2O_7^{2-}$) depending on the pH [5].

Cr(VI) is widely used by different industries like metalworking industry (electroplating, metal refining, refractories…), textile industry (textile dyeing, pigment production…) and other industrial activities such as fungicide production or leather tanning. Tanning industry is one of the most chromium-emitting. Chromium compounds are also used in small amounts for many industrial products such as corrosion inhibitor, military aircraft, catalysts… [5].

Cr(VI) is the most toxic species among its different oxidation states. It is considered a "human carcinogen" by the US EPA and the World Health Organization. It is also associated with other pathological effects such as genotoxicity, mutagenicity and dermatotoxicity. It may cause respiratory, cardiovascular, and gastrointestinal diseases, and it is related to reproductive and developmental pathologies. Cr(VI) is also toxic to aquatic animals, plants, and bacteria. Cr(III) is 100 times less toxic than Cr(VI). In humans and in small quantities, chromium is an essential nutrient required for sugar and lipid metabolism, but in excess it may cause cancer and allergic skin reactions [5–7].

Wastewaters which contain Cr(VI) must be treated before being dumped into the aquatic system due to its toxicity. The most common

* Corresponding author.
E-mail address: jose.barriada@udc.es (J.L. Barriada).

https://doi.org/10.1016/j.jece.2022.108258
Received 18 April 2022; Received in revised form 22 June 2022; Accepted 10 July 2022
Available online 12 July 2022

method for Cr(VI) removal is acid reduction to Cr(III) and its subsequent precipitation as hydroxide by increasing pH with lime. The main disadvantage of this method is the removal of the large solid wastes produced. Different technologies have been studied for chromium elimination because of this disadvantage, such as ion exchange, membrane technologies or adsorption. Adsorption is a technique with high versatility which is being widely studied for pollutant elimination. One of the most used adsorbents is activated carbon [8], but it is expensive so during the last years, many studies of sorption with low-cost sorbents have been developed [6,9].

Low-cost materials like marine biomass or iron (Fe) nanoparticles have provided good results in the removal of different metals [10–14]. In the case of iron nanoparticles, despite providing good results, their main disadvantage is their separation from the reaction medium after use. One of the most common ways to solve this problem is to synthetize magnetic nanoparticles [15–17] but other problems such as agglomeration of these particles remain. Adsorption of iron on a solid support is another way of being able to remove active material after the decontamination process without losing the decontamination properties of the nanoparticles. In addition, these materials have the advantage that they can be easily used as fillers in adsorption columns. Our research group has studied iron and biomass immobilization in silica gel obtaining good results in metal removal [18]. Silica gel is a material which presents optical transparency and high porosity combined with a good mechanical resistance. Porosity allows the solution to penetrate in the silica gel, increasing the surface where iron could be adsorbed, which implies more iron available for the decontamination process. This structure combined with a large amount of oxygen in the crystal lattice allows silica gel to have a high affinity for metal cations depending on its charge and size. In this work, silica gel was synthetised in the form of pellets by a sol-gel process using the aqueous precursors method [15]. We have checked that this Supporting material does not interact with chromium solutions, so we have functionalised it by treatment with an iron solution. Iron is the metal chosen to immobilize over silica gel because it has provided good results for chromium elimination [19]. We have studied the process of iron retention on the surface of the Supporting material. Besides, the immobilization over a solid surface method also facilitates the possibility of modifying the iron to further improve chromium removal. Modification could be carried out with chemical modifiers but, as an alternative, we have chosen the extract obtained from eucalyptus leaves to follow a more sustainable process [15,16].

2. Materials and methods

2.1. Chemicals

Reagents used to synthesize silica pellets were sodium silicate neutral solution, pure from Scharlau (Scharlab S.L., Barcelona, Spain) and HCl 37 % PA-ACS-ISO. Iron sulphate 7-hydrate PA-ACS, potassium dichromate PA-ACS-ISO from Panreac (Panreac Química S.A., Barcelona, Spain) and chromium (III) chloride hexahydrate from Sigma (Sigma-Aldrich, Steinheim, Germany) were used to prepare metal solutions. Iron measurements were performed using 1,10-phenantroline 1-hydrate PA-ACS, acetic acid glacial purissimum, sodium acetate 3-hydrate (RFE, USP, BP Ph. Eur.) and hydroxylammonium chloride (ACS, ISO) from Panreac. Cr(VI) determination was performed using 1,5-diphenylcarbazide ACS from Sigma-Aldrich and H_2SO_4, 95–97 % expertQ, ISO from Scharlau. All solutions were made with deionised water. pH was adjusted with HCl and NaOH 98 % ACS-ISO from Panreac.

2.2. Materials

The biomaterial used in this work (eucalyptus leaves) was collected in Galicia (Spain). Eucalyptus extract was prepared following the method described by Martinez-Cabanas et al. [15]. In brief the extract was prepared by reflux in deionised water with ground eucalyptus leaves for 40 min and a subsequent vacuum filtration. A full description of the process can be found at the reference provided. Further characterization of the extract provided the following parameters: pH $= 4.2 \pm 0.2$, reduction potential $= 221{,}6 \pm 6.1$ mV with respect to an Ag/AgCl 3 M reference electrode, conductivity $= 430 \pm 3$ μS·cm^{-1}, turbidity $=$ 54 NTU, organic carbon $= 2082 \pm 73$ mg/L.

2.3. Synthesis and functionalization of silica pellets

The synthesis process of silica gel pellets is an adaptation of the method described by Martinez-Cabanas et al. [18]. 30 ml of 1.8 M Na_2SiO_3 solution was mixed with 30 ml of H_2O. Then 3.6 ml of 4 M HCl was added to neutralize the solution. The mixture was stirred until polymerization began. Then, the formed gel was poured into a home-made acrylic glass mould with holes of 7 mm in diameter and 5 mm in heigh. These gel pellets were dried on a stove (Memmert beschickung-loading model 100–800) for 24 h at 25 ºC. As a result, in hard and stable pellets are obtained. This material was designated as GSP.

GSP was loaded with iron by a sorption process. About 0.3 g of GSP pellets were added to 50 ml of 250 mg·L^{-1} Fe(II) solution in 100 ml conical flasks. Several flasks were prepared and agitated on a rotatory shaker (Edmund Bühler KS-15) for 24 h at 175 RPM and room temperature. After this step, GSP pellets were removed from the solution by decantation. Pellets were dried for 24 h. This material was designated as GSP-Fe.

GSP-Fe pellets were further treated before using it for decontamination process. The treatment was performed submerging the material in a eucalyptus extract for 20 h at room temperature. Then pellets were rinsed twice with deionised water. This material was designated as GSP-Fe(0).

2.4. Materials characterization

Different experiments were carried out to characterize the material. Scanning Electron Microscope (SEM) and Energy Dispersive X-Ray Spectroscopy (EDS) tests were done to GSP, GSP-Fe, GSP-Fe(0) pellets, and to GSP-Fe pellets after 2 elimination cycles, to examine the surface of the material and the distribution of adsorbed metals. N_2 adsorption test were done to determine the surface area and porosity. XPS analyses were also done to GSP-Fe and GSP-Fe(0) to further characterize iron oxidation state. Iron concentration in solution was determined after treating the solution with a standard reduction method to reduce Fe(III) to Fe(II) [20] using $NH_2OH{\cdot}HCl$. An UV–VIS spectrophotometry standard method was used for iron measurements (Zuzi spectrophotometer model 4211/20) at 510 nm [20].

2.5. Effect of pH

pH effect was tested on iron sorption, Cr(VI) elimination and total chromium sorption. pH of all solutions was adjusted with HCl or NaOH solutions as required. Effect on iron sorption was performed by addition of 0.1 g of GSP pellets to 50 ml of 25 mg·L^{-1} Fe(II) solutions in conical flasks. pH was adjusted between 1 and 6. Flask were stirred for 24 h and 175 RPM at room temperature. The effect on Cr(VI) elimination was performed by addition of 0.1 g of GSP-Fe(0) pellets to 50 ml of 100 mg·L^{-1} Cr(VI). pH was adjusted between 1 and 5. Chromium (VI) measurements were performed by a UV–VIS spectrophotometry standard method at 540 nm [21]. Total chromium was also determined by flame absorption (FAAS) (Varian SpectrAA-55B) at 428.9 nm.

2.6. Kinetic studies

Iron sorption equilibrium time was determined by addition of 0.2 g of GSP pellets to 100 ml of 85 mg·L^{-1} Fe(II) solution. Experiments were

done at room temperature, natural pH (ca. pH 5), and stirring during 24 h. Chromium equilibrium time was determined with 0.4 g of GSP-Fe(0) pellets and 100 ml of 75 mg·L^{-1} chromium solution. Experiments were performed at room temperature, pH = 1 and stirring during 24 h.

2.7. Equilibrium studies

Effect of initial concentration on iron sorption and chromium elimination was also analysed. 0.1 g of GSP pellets were added to 50 ml Fe(II) solution. Several solution concentrations were tested ranging from 40 to 125 mg·L^{-1}. Experimental conditions were the same than in the kinetic studies. Similarly, chromium equilibrium studies were performed adding 0.2 g of GSP-Fe or GSP-Fe(0) pellets to several 50 ml chromium solutions with concentrations between 10 and 300 mg·L^{-1}.

The effects of temperature and ionic strength on Cr(VI) removal and total chromium adsorption have also been studied. 0.2 g of GSP-Fe(0) pellets were added to several 100 ml of 100 mg/L Cr(VI) solutions. The elimination process was performed at different temperatures (from 10 to 52 ºC). In ionic strength studies, 0.2 g of GSP-Fe(0) pellets were added to several 100 ml of 100 mg/l Cr(VI) solutions with ionic strengths from 0.05 M to 0.5 M. Ionic strength was adjusted using KNO_3 as electrolyte.

2.8. GSP-Fe(0) service life studies

GSP-Fe(0) service life was studied by using the material in elimination process with subsequent Fe(0) regeneration with eucalyptus extract. 0.2 g of GSP-Fe(0) pellets were added to a 50 ml Cr(VI) solution. After the Cr(VI) elimination process, pellets were rinsed with deionised water and submerged in the eucalyptus extract as it is described in Section 2.3 to use them in a new elimination process. This procedure was repeated in three complete elimination processes.

3. Results and discussion

3.1. Materials characterization

The first material synthetised, GSP, is snow-white in colour and powdery in appearance. GSP pellets have a diameter from 4 mm to 5 mm and a thickness from 1 mm to 1.5 mm. In the SEM image of this material (Fig. 1a) it can be seen that pellets have a rough surface. EDS analysis shows that this roughness is related to the presence of NaCl from the reaction between the Na_2SiO_3 and HCl used in the synthesis of the material. NaCl is deposited on the polymerised silica gel structure (Fig. 2).

GSP was studied as a Cr(VI) adsorbent. GSP pellets were placed in contact with Cr(VI) solutions at different concentrations. The adsorption values ranged from –0.58 mg Cr(VI)/g GSP to 0.46 mg Cr(VI)/g GSP. So, adsorption on GSP was negligible. Consequently GSP was transformed by functionalisation with Fe(II). The resulting material, called GSP-Fe, has a distinct reddish-brown colour and its surface is no longer powdery in appearance. The pellet size of this second material is also smaller, approximately 3 mm in diameter and 1 mm thick. The SEM image (Fig. 1b) shows a clear difference from the GSP shown in the Fig. 1a. The pellet surface does not have the same roughness, and in addition, there are plenty of small formations attached to the surface. The EDS analysis associates these formations to the Fe adsorbed on the pellet (Fig. 3a, b). EDS also show that there is no NaCl in the GSP-Fe, so it can be concluded that it is washed away in the Fe(II) solution used to functionalise the material. This is consistent with the decrease in the

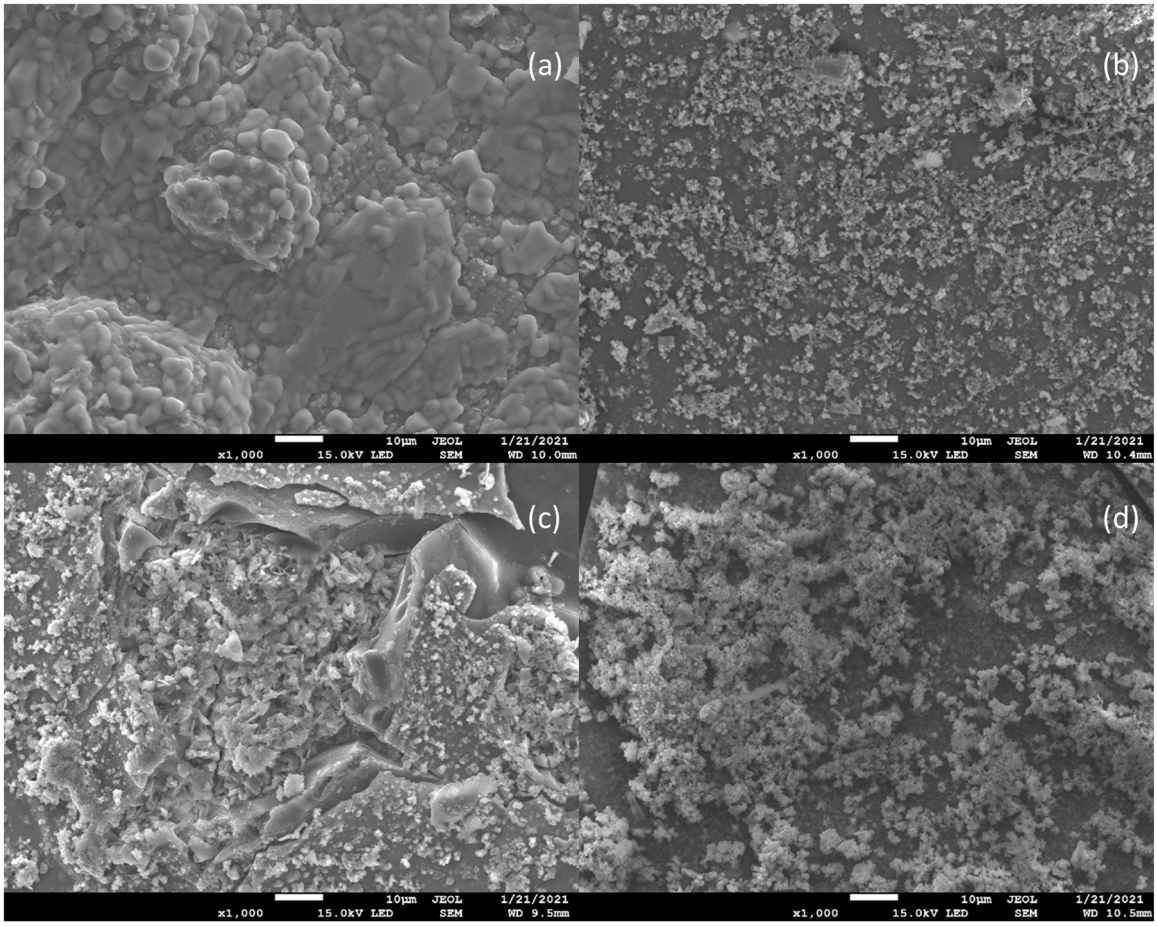

Fig. 1. SEM images of GSP (a), GSP-Fe (b), GSP-Fe(0) (c) and GSP-Fe after two elimination cycles (d).

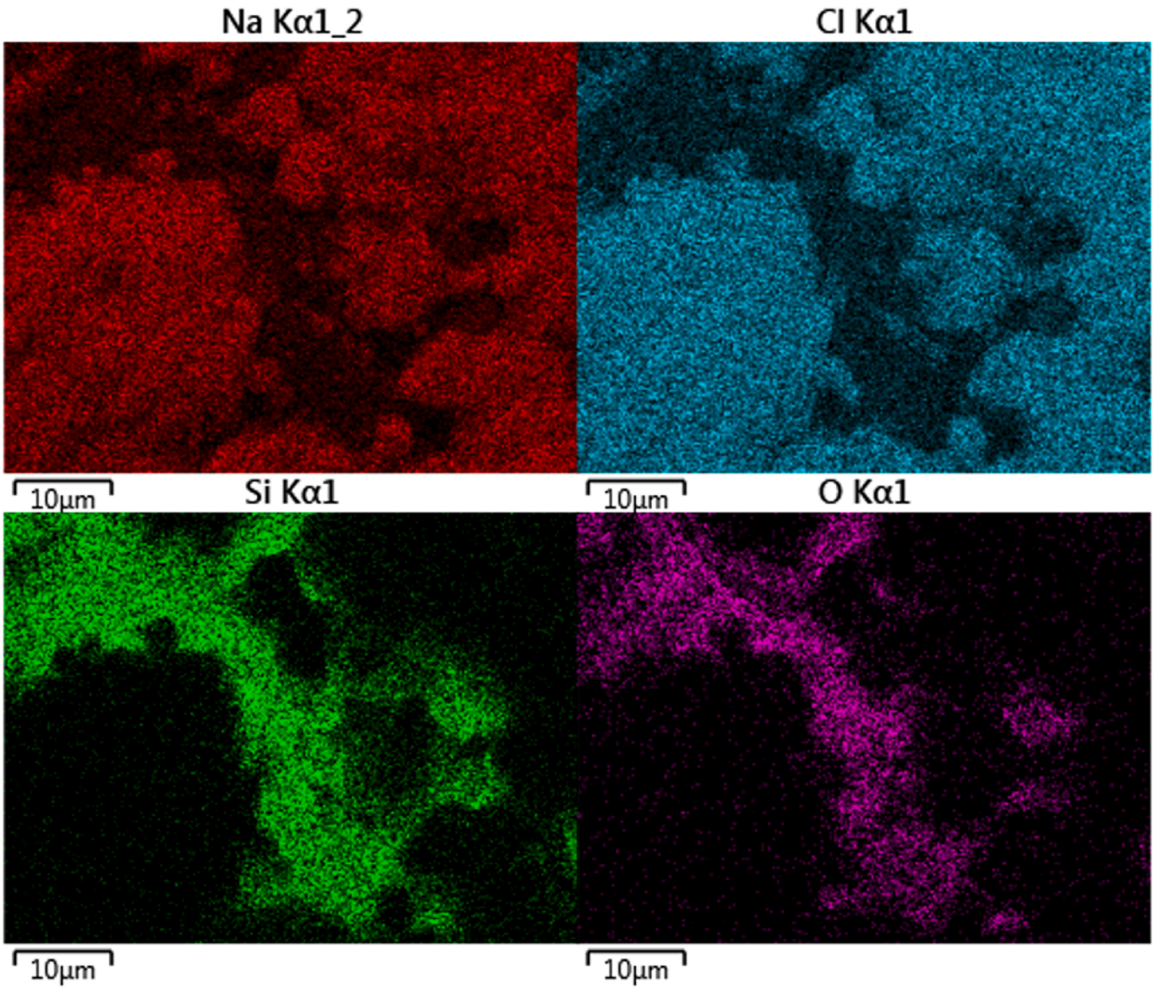

Fig. 2. EDS images of GSP. Coloured zones indicate the presence of each element. Na (red), Cl (cyan), Si (green), O (purple).

pellet size that occurs during the functionalisation process.

GSP-Fe was studied as a Cr(VI) remover and in this case, Cr(VI) adsorption was observed. The results of these studies are discussed in Section 3.2. However, to increase the amount of Cr(VI) removed, a second modification was made to the GSP-Fe by treating this material with a eucalyptus extract. The material obtained, GSP-Fe(0), has a dark, almost black colour. In contrast to what happened during the GSP functionalisation process, GSP-Fe(0) has the same pellet size as GSP-Fe. In addition the iron formations show no significant differences between Fig. 1b and c. Fig. 3c and d also show no significative changes from those shown in, Fig. 3a and b. This black colour is different from the colour of the material when the iron adsorbed on the material is mainly Fe(III) (reddish-brown) or when it is Fe(II) (blue-cyan). Black colour is also obtained when chemical reductants such as $NaBH_4$ are used instead of eucalyptus extract. These observations, together with the black colour (characteristic of Fe(0)), are an indication that the eucalyptus extract acts as a natural reductant, reducing the iron to Fe(0) without altering the surface of the material. This fact agrees with the reduction capacity of this extract discussed in the bibliography [15] and with the experimental data obtained from the extract (Section 2.2). Another experimental evidence for the presence of Fe(0) in the material is that GSP-Fe (0) acts as a reductant in the Cr(VI) process described in Section 3.3.3, while GSP-Fe does not.

Fig. 1d, which corresponds to the material after the Cr(VI) elimination process, is significantly different from Fig. 1c. The formations observed on the silicate surface have an agglomerated appearance. The EDS analysis performed to this material (Fig. 4) indicates the presence of both iron and chromium in the silicate surface. Chromium is preferentially associated to iron spots because of the density of signals corresponding to chromium is more important in those locations where iron is present.

N_2 sorption test were done using GSP-Fe(0) and GSP-Fe(0) after de Cr (VI) elimination process. The N_2 adsorption and desorption experimental data conform to a type 4 isotherm among those described by Brunauer et al. [22,23]. GSP-Fe(0) has a Brunauer–Emmett–Teller (BET) surface area of 481.8 $m^2 \bullet g^{-1}$ and a pore volume of 0.55 $cm^3 \bullet g^{-1}$. After the elimination process the values are very similar. A BET surface area of 489.2 $m^2 \bullet g^{-1}$ and a pore volume of 0.57 $cm^3 \bullet g^{-1}$ were found in the material.

Further information like optical images of all the synthetised materials (GSP, GSP-Fe, GSP-Fe(0), more SEM images and EDS analyses, N_2 adsorption figures and further parameters can be found in the Supplementary material.

3.1.1. *Characterization of the iron of GSP-Fe and GSP-Fe(0)*

XPS analyses were done to GSP-Fe, GSP-Fe(0) and GSP-Fe(0) after Cr (VI) elimination. The main difference in the spectra of the three materials is that the C 1 s signal in GSP-Fe(0) spectrum (Fig. 5a, red) is much higher than in the other spectra. The organic material present in the GSP-Fe(0) plays an important role in the stability of the material, which is described in more detail in Section 3.2.1. The Fe characterization of the materials is shown in Fig. 5b, c, and d. Table 1 summarises the ratios of the oxidation states of iron in the materials.

In GSP-Fe the main oxidation state is Fe(III) (Fig. 5b). However, this

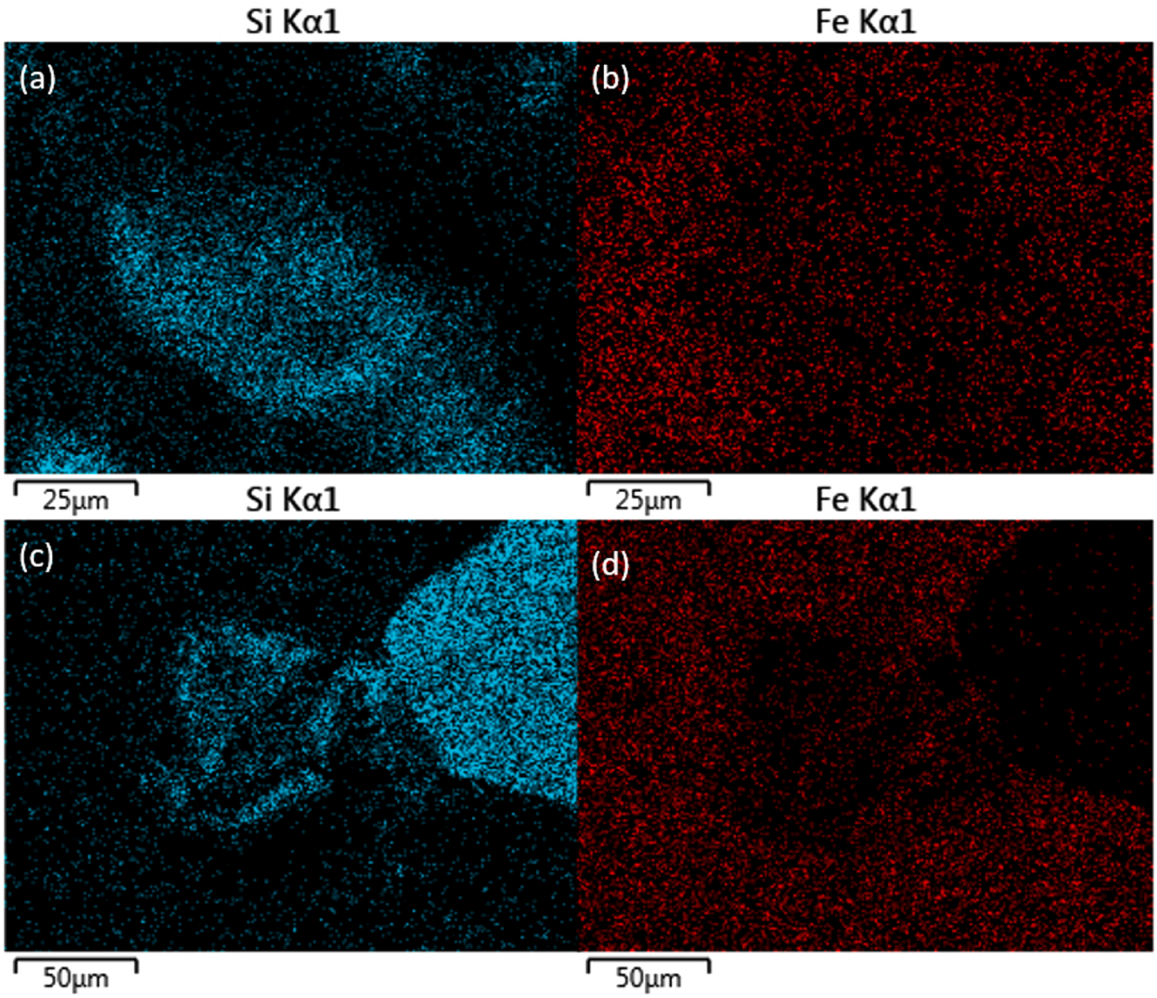

Fig. 3. EDS images of GSP-Fe (a, b) and GSP-Fe(0) (c, d). Coloured zones indicate the presence of each element. Si (cyan), Fe (red).

material was prepared using $FeSO_4$ so when the GSP is immersed in the $FeSO_4$ solution, a very fast oxidation of Fe(II) to Fe(III) occurs on the surface of the silica gel.

An adsorption process of Fe(II) on GSP in an inert N_2 atmosphere was carried out to confirm this oxidation. In this case, the GSP-Fe obtained did not show the reddish-brown colour but had a blue-cyan coloured surface. After removal of the inert atmosphere, the colour of these pellets turned reddish in a few hours, confirming that iron is oxidised on the surface of the silica gel owing to the presence of O_2 dissolved in the $FeSO_4$ solution.

The XPS of GSP-Fe(0) shows that after the treatment with the eucalyptus extract there is a change in the oxidation state of iron. However, in the XPS spectrum (Fig. 5c), the peak corresponding to Fe(0) which appears between 706 and 707 eV was not observed. This could be because XPS is a surface technique, which goes from 2 to 5 nm deep. GSP-Fe(0) is a material in which the surface Fe(0) is easily oxidised, so the technique only finds the already oxidised iron. Even so, the analysis shows that there is a reduction of the iron present in the material, and there is experimental evidence to support that the extract reduces iron to Fe(0).

Finally, after the Cr(VI) removal process the iron is oxidised again, being Fe(III) the main oxidation state (Fig. 5d). The organic signal of the material also decreases. This indicates that the reduction process carried out by the extract is reversed.

3.2. Studies of the iron sorption on GSP: kinetics and equilibrium

As it has been mentioned in the previous section, iron is key for the chromium elimination process, so the interaction between iron and GSP was further studied by reaction kinetics, pH dependency, adsorption isotherms and stability assays.

Kinetic studies were performed to establish iron sorption equilibrium time. Most of the iron sorption (80 %) occurred in the first 5 h and equilibrium was reached in 15 h. Considering these observations, we decided to keep the reaction during 24 h for the iron loading process to ensure maximum iron sorption. Kinetics were fitted using a pseudo-second order model [24] with the following expression

$$c = c_o - \frac{q_e^2 kt}{(1 + kq_e t)} * \frac{m}{V} \quad (1)$$

where c is the metal concentration at time t in $mg{\cdot}L^{-1}$, c_o is the initial metal concentration ($mg{\cdot}L^{-1}$), q_e is the sorption capacity at equilibrium in $mg{\cdot}g^{-1}$, t is the time in h, m is the sorbent mass in g, V is the solution volume in L and k represents the pseudo-second order rate constant ($g{\cdot}mg^{-1}{\cdot}h^{-1}$). Pseudo-second order parameters are shown in Table 2 and the kinetics plot can be found in the Supplementary material. This fitting model was chosen because it is commonly used in adsorption studies providing good results, and it correctly fits the experimental data.

After the determination of the equilibrium time for iron sorption, pH dependence studies were performed to find out the conditions of the maximum iron sorption capacity. Natural pH of the iron solution with GSP ranges from 5.4 at [Fe(II)] $= 50\ mg{\cdot}L^{-1}$ to 5 at [Fe(II)]

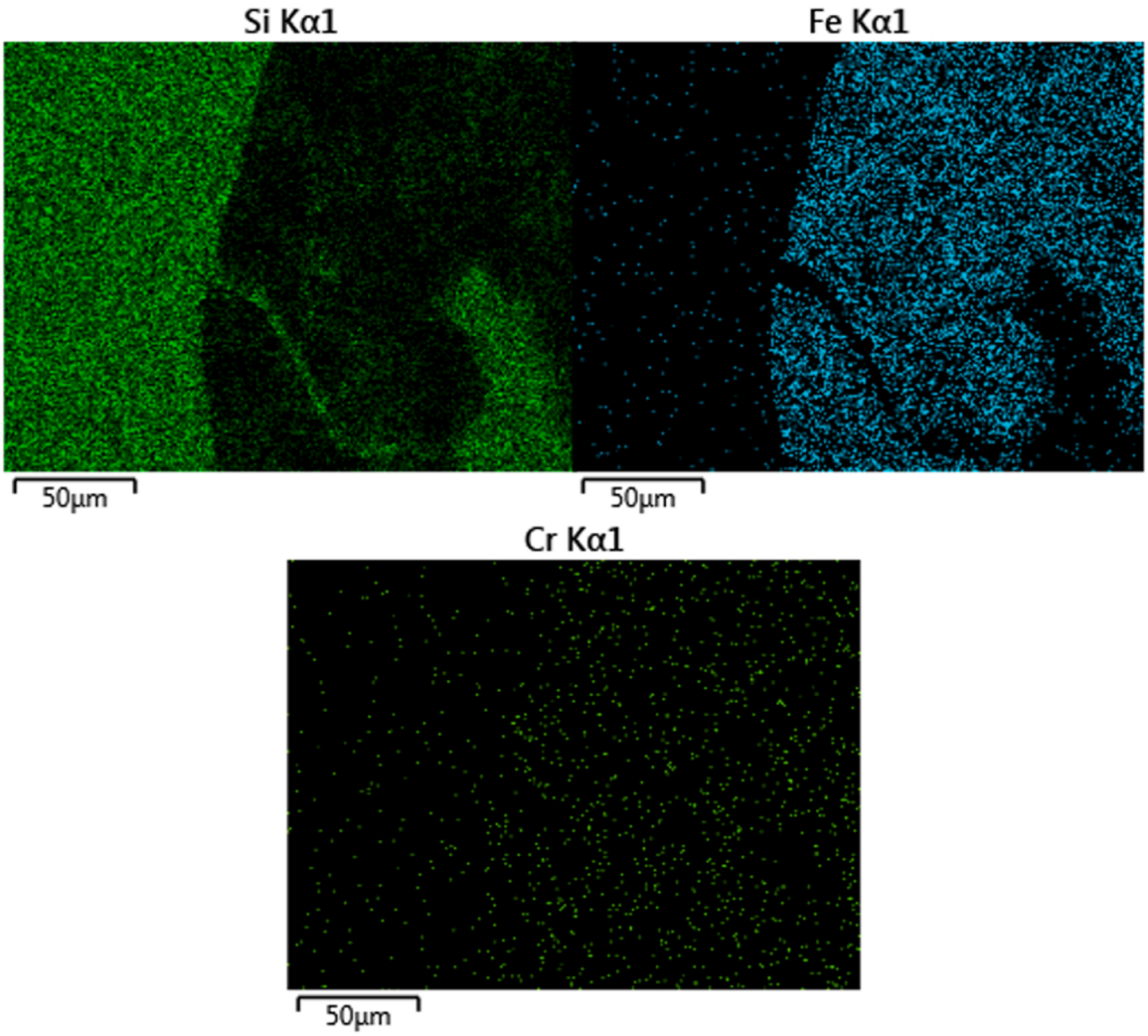

Fig. 4. EDS images of GSP-Fe(0) after two elimination cycles. Coloured zones indicate the presence of each element. Si (green), Fe (cyan), Cr (yellow - green).

= 250 mg·L^{-1}. As Fig. 6a shows, above pH 4, adsorption increases strongly as pH increases. This fact could be explained by the protonation of oxygens of the GSP surface at low pH values. A high concentration of protons prevents iron from being retained on the surface by interaction with the oxygens. When pH is above 6, iron begins to form hydroxides [25] which precipitate in the reaction medium, so no iron is available to be adsorbed onto the GSP pellets. Natural pH conditions (from 5.4 to 5) provide high sorption without the hydroxide formation problem, so these conditions were selected to continue the experiments on iron sorption.

Finally, equilibrium studies were performed to determine the material sorption capacity. The sorbent materials employed in this study were prepared as pellets. This arrangement makes extremely difficult weighing the same amount of material twice with the precision require in adsorption experiments. This difference in weight would affect to both the concentration of adsorbate at equilibrium and the amount of pollutant removed from solution (i.e., x-axis variable and y-axis variable in an isotherm plot). All the equilibrium experiments were done duplicating the isotherms at different concentrations to overcome this problem, rather than trying to duplicate the weight of sorbent. Those isotherms duplicates have been represented in one single plot, showing in all cases the same isotherm trend between duplicates.

Experimental data were fitted using Langmuir model, Langmuir-Freundlich model and the model described by Sellaoui et al. [26] for a monolayer sorption and one energy site:

$$q = \frac{Q_o}{1 + (c_{½}/c)^n} \quad (2)$$

where q is the metal amount adsorbed at equilibrium time in mg·g^{-1}, Q_o is the maximum adsorption capacity (mg·g^{-1}), c is the equilibrium metal concentration in the solution (mg·L^{-1}), $c_{½}$ is the concentration at half saturation of the material (mg·L^{-1}) and n is the number of atoms per adsorption site. Fig. 6b shows the fitting curve, and fitting values are summarised in Table 3. The three models provide similar Q_0 values, being equal in the Langmuir-Freundlich and Sellaoui models. Iron sorption by GSP (24.5 mg·g^{-1}) is more efficient than iron adsorption by commercial silica (2.31 mg·g^{-1}) [27]. As Fig. 6b shows, GSP has a very high affinity for iron which is observed by the nearly vertical slope before saturation. The material presents a good adsorption capacity and reaches saturation with low iron concentrations. This is a remarkable behaviour, because it allows the functionalisation of GSP with low Fe(II) concentration solutions, minimising the waste of Fe(II) in the process. This high affinity also allows iron to remain adsorbed during the decontamination process. Adsorption energy is an indication of the affinity between adsorbent and adsorbate. This value can be related to the concentration at half saturation and to the solubility (c_s) of the adsorbate according to the following Equation [28]:

$$E = RTln\frac{c_s}{c_{½}} \quad (3)$$

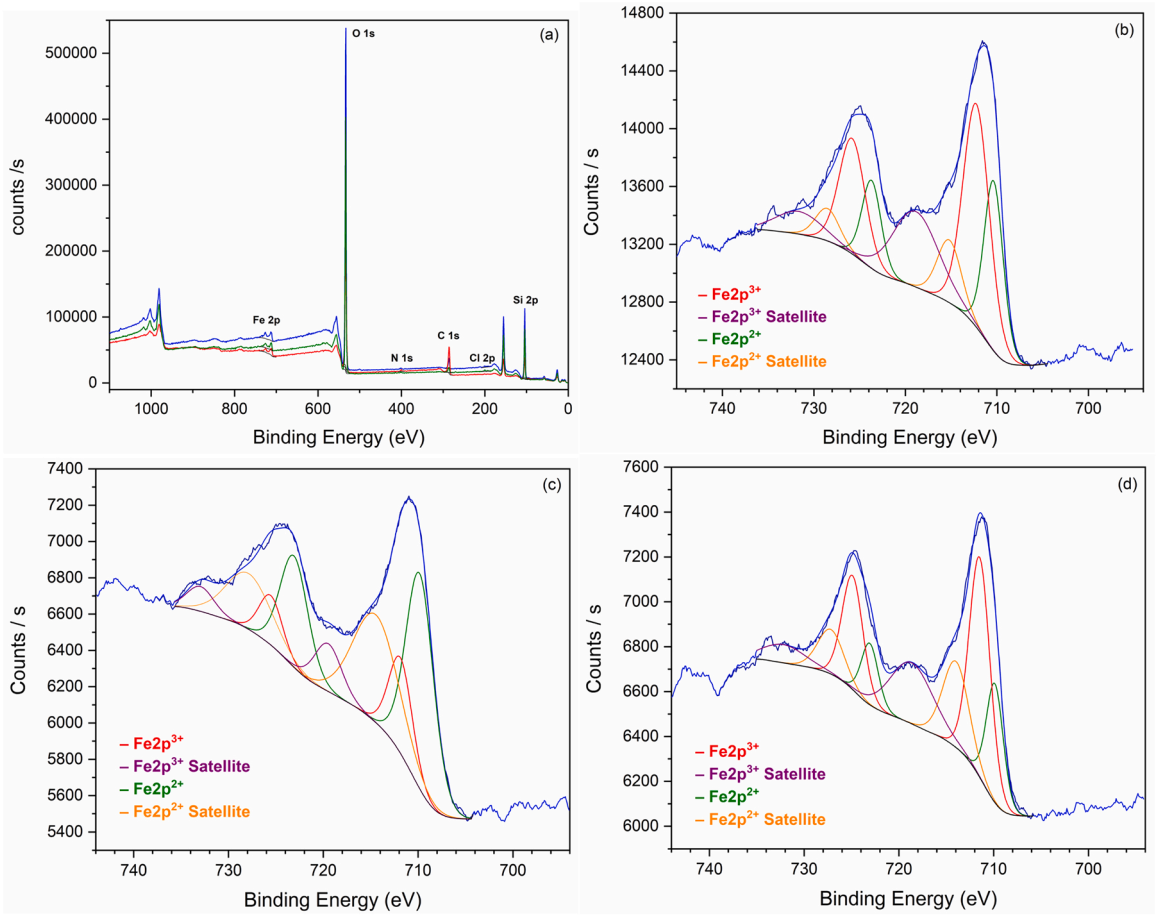

Fig. 5. a) Whole XPS spectra of GSP-Fe (blue), GSP-Fe(0) (red) and GSP-Fe(0) after Cr(VI) removal (green). b – d) XPS iron signals of GSP-Fe (b), GSP-Fe(0) (c) and GSP-Fe(0) after Cr(VI) removal (d). For b – d: Fe2p^{3+} (red), Fe2p^{3+} satellite (purple), Fe2p^{2+} (green), Fe2p^{2+} satellite (orange).

Table 1
Fe oxidation states of the materials synthesised in this work provided by XPS analyses.

Oxidation State	GSP-Fe		GSP-Fe (0)		GSP-Fe (0) after Cr (VI) removal	
	Peak BE	Relative %	Peak BE	Relative %	Peak BE	Relative %
Fe2p Fe^{2+}	710.36	23.22	709.83	41.51	709.87	17.59
Fe2p Fe^{3+}	712.25	41.54	711.86	15.48	711.48	40.03
Fe2p Fe^{2+} Satellite	715.2	10.66	714.45	34.03	713.98	19.5
Fe2p Fe^{3+} Satellite	718.87	24.58	719.48	8.98	718.65	22.87
Fe^{3+}/ Fe^{2+} Ratio		1.952		0.324		1.696

Table 2
Kinetic parameters obtained from pseudo-second order fitting of iron sorption (Figure S 5) and Cr(VI) elimination (Figure S 6). Figures can be found in the Supplementary material.

Kinetic parameters			Pseudo second order model		
Element	c_o ($mg \bullet L^{-1}$)	pH	q_e ($mg \cdot g^{-1}$)	k ($g \cdot mg^{-1} \cdot h^{-1}$)	R^2
Iron	85	Nat.	27.0 ± 0.3	$19.4 \bullet 10^{-3} \pm 1.0 \bullet 10^{-3}$	0.993
Cr(VI)	75	1	246 ± 4	$115 \bullet 10^{-3} \pm 9 \bullet 10^{-3}$	0.989

The c_s values used for the energy calculations were provided by the reagent manufacturer ($FeSO_4$ = 400 $g \cdot L^{-1}$, $K_2Cr_2O_7$ = 115 $g \cdot L^{-1}$). As Table 3 shows, adsorption energy of iron with GSP is important, larger than that found for other types of compounds adsorbed on similar supports (6.18–12.0 $kJ \cdot mol^{-1}$) [29], or other polymeric materials (19.71–33.22 $kJ \cdot mol^{-1}$) [28]. This large adsorption energy agrees with the high affinity of GSP for Fe shown in Fig. 6b. The adsorption energy value is less than 40 $kJ \cdot mol^{-1}$, indicating that the adsorption process of Fe on GSP is a physisorption process [30].

The amount of iron adsorbed on GSP-Fe was confirmed by desorption using concentrated HCl (pH < 1). The mass of iron desorbed (24.8 ± 0.6 mg Fe/g GSP-Fe) was consistent with the value of iron adsorbed on GSP-Fe obtained from the adsorption isotherm (24.5 ± 0.2 mg Fe/g GSP-Fe).

Further information, such as the Fe(II) sorption experimental data fitted using the Langmuir and Langmuir-Freundlich models can be found in the Supplementary material.

3.2.1. *Stability of GSP-Fe(0) and GSP-Fe*

Stability of the materials was tested in different solutions. 0.2 g of GSP-Fe(0) was submerged into 50 ml of deionised water, 50 ml of deionised water acidified with different acids (HCl, H_2SO_4) up to pH 1, and 50 ml mixtures of deionised water and commercial acids (HCl, H_2SO_4, HNO_3, 50 % water and 50 % of the commercial acid). Flasks were stirred at 200 RPM in a rotatory shaker. After a week, GSP-Fe(0) pellets submerged in deionised water did not undergo any change, while the GSP-Fe(0) pellets submerged in the pH 1 HCl solution recovered the reddish-brown colour, characteristic of GSP-Fe material. Total Fe of the deionised water flask and pH 1 HCl flask was measured. Results

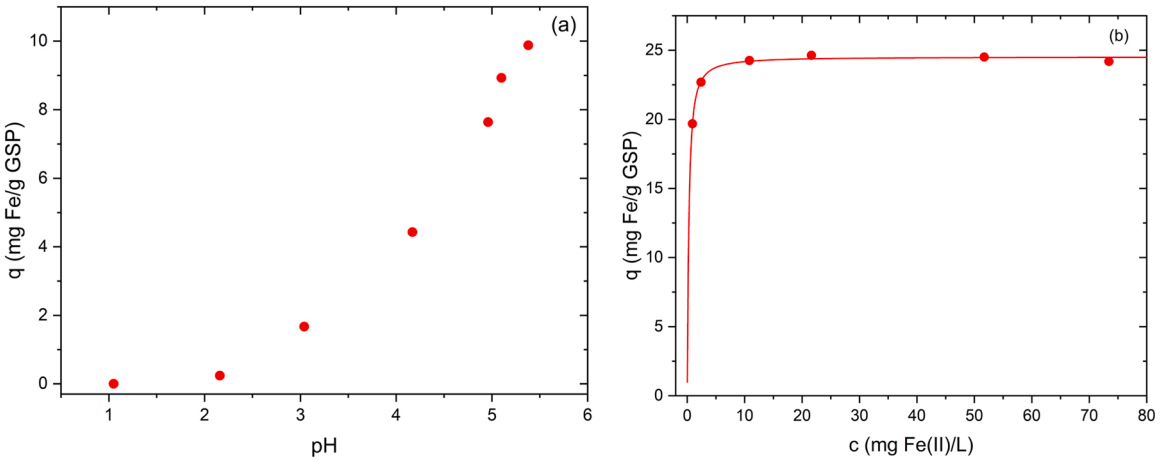

Fig. 6. (a) pH dependence of Fe sorption on GSP. Material dose 2 g·L^{-1} and room temperature. Fe(II) initial concentration: 25 mg·L^{-1}. (b) Equilibrium experimental data of Fe sorption on GSP. Material dose 2 g·L^{-1}, natural pH (5.4–5) and room temperature. Solid line was obtained by fitting to Eq. 2.

Table 3
Equilibrium fitting parameters for the metals studied. Qo represents the maximum adsorption capacity; The last column is referred to the Cr(VI) amount that the GSP-Fe(0) can remove from the solution by the full reduction and adsorption process.

Isotherm model		Fe (II) Sorption	Cr (VI) Sorption	Total Cr Sorption	Cr (VI) Elimination
Langmuir	Q_o (mg•g^{-1})	24.65 ± 0.13	106 ± 6	282 ± 8	–
	b (L•mg^{-1})	4.5 ± 0.3	9.7•10^{-3} ± 1.3•10^{-3}	14.9•10^{-3} ± 1.1•10^{-3}	–
	R^2	0.983	0.991	0.996	–
Langmuir-Freundlich	Q_o (mg•g^{-1})	24.52 ± 0.15	154 ± 32	279 ± 18	–
	b (L•mg^{-1})	3.5 ± 0.6	4•10^{-3} ± 2•10^{-3}	15•10^{-3} ± 2•10^{-3}	–
	n	0.83 ± 0.12	1.33 ± 0.14	0.98 ± 0.09	–
	R^2	0.985	0.997	0.995	–
Sellaoui (Eq. 2)	Q_o (mg•g^{-1})	24.5 ± 0.2	153 ± 32	279 ± 18	–
	n	1.2 ± 0.2	0.75 ± 0.08	1.02 ± 0.09	–
	$c_{1/2}$ (mg•L^{-1})	0.28 ± 0.05	256 ± 139	65 ± 10	–
	R^2	0.985	0.997	0.995	–
	E (kJ•mol^{-1})	34.5	14.9	–	–
Elimination by the full process (Reduction-adsorption)	Q_o (mg•g^{-1})	–	–	–	383 ± 16

showed that less than 1 % of the iron adsorbed in the pellets was released to solution, so the material is very robust in the experimental solution.

On the contrary, GSP-Fe(0) was not stable in H_2SO_4 solution. After 12 h in a pH 1 solution, pellets lost the reddish-brown colour gained during the iron load. This fact happened faster when the acid concentration increased. The material was also unstable in concentrated HCl and HNO_3, but the degradation process was slower than in H_2SO_4.

GSP-Fe is stable in deionised water, but in a pH 1 HCl solution it also loses the characteristic iron colour after two days. This difference in stability indicates that during the treatment with the eucalyptus extract, where GSP-Fe is transformed to GSP-Fe(0), an organic matter layer is formed on the pellets. These organic compounds retained in the GSP-Fe

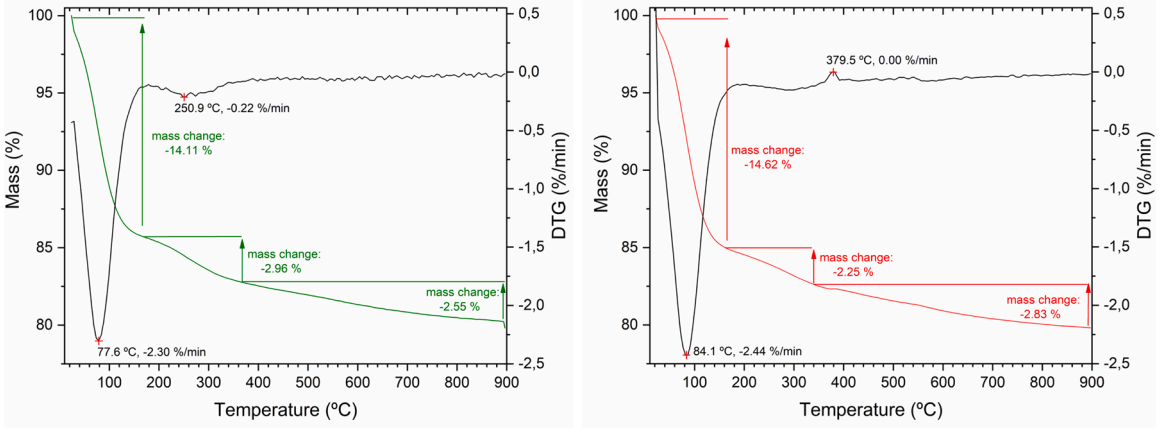

Fig. 7. TGA graphs of GSP-Fe(0) decomposition in O_2 (left, green) and N_2 (right, red) and DTG (derivative thermogravimetry, black).

(0) pellets act as capping agents, which contributes to stabilise the iron fixed on the material in acidic media. Analyses performed to aqueous extracts of eucalyptus indicate that there are a wide variety of compounds in its composition [31,32] (eucalyptol, pinene, 1,8-Cineole, among many others). Using the Folin-Ciocalteu method it was found that that these compounds include significant number of polyphenols, and by measuring the DPPH Radical Scavenging Capacity, it was observed that the compounds present in the extract possess antioxidant activity [33,34]. These compounds are the responsible of the reduction of iron in the silica gel pellets.

A Thermogravimetric Analysis (TGA) was carried out to check and quantify the presence of organic matter on the GSP-Fe(0) pellets (Fig. 7). The TGA graph presents an indicative slope of multi-step decomposition. In a first step, between 20 ºC and 170 °C, a mass decrease of about 14 % is observed in both inert and oxidant atmosphere, associated with water loss. In a second step, between 170 ºC and 340–360 ºC, a mass loss of about 3 % in the presence of oxygen and 2 % in the presence of nitrogen is observed. This mass loss is associated to decomposition of organic matter by combustion in presence of oxygen and by pyrolysis in presence of nitrogen. The IR gas analyses confirm this hypothesis. Within this temperature range, in the presence of oxygen, O═C═O stretching signals appear at 2360 and 2321 cm^{-1} [35,36]. Those signals are not present in an inert atmosphere (N_2). In addition, XPS analysis of GSP-Fe (0) confirms the existence of organic matter in the material.

The results support our suggestion that organic matter plays an important role in GSP-Fe(0) stability and confirm that the green synthesis approach is key in the preparation of a stable and functional material.

3.3. Chromium elimination studies: kinetics and equilibriums

3.3.1. Cr(VI) interaction with GSP

Experiments were designed to eliminate as much as possible of the most toxic chromium species, that is Cr(VI). During the equilibrium studies using GSP, no Cr(VI) sorption was observed. This fact confirms that the GSP role in the removal process is only to retain iron immobilised in its surface and it does not interact with chromium. Immobilised iron is the species that reacts with chromium in the elimination process. For this reason, equilibrium experiments of chromium elimination were studied, and they were referred to iron present in the pellets.

3.3.2. Cr(VI) sorption by GSP-Fe

Cr(VI) sorption was studied using GSP-Fe. Fig. 8a shows the experimental data fitted using Eq. 2, and the maximum sorption capacities (Q_o) for Cr(VI) of the three isotherm models (Langmuir, Langmuir-Freundlich and Sellaoui model) are shown in Table 3. In this case, the Langmuir model provides a value of Q_0 different from the value provided by the Langmuir-Freundlich model and the Sellaoui model. Moreover, although Langmuir-Freundlich and Sellaoui models describes properly the experimental data, they give a large error in the Q_o parameter because the saturation zone of the isotherm is clearly not reached. The large error obtained in the parameters $c_{½}$, and b is also associated with the absence of a saturation of the material. The $c_{½}$ parameter is defined as the concentration of adsorbate in solution when the adsorbent has half of the adsorption positions occupied, so if the saturation zone is not reached, this parameter cannot be calculated accurately. The parameter b in the Langmuir-Freundlich model is the reciprocal of $c_{½}$. Sorption energy (Table 3) was calculated using Eq. 3. Fig. 8b shows the Cr(VI) elimination percentages in solutions with different Cr(VI) concentrations. As we mentioned in the previous section, no Cr(VI) sorption was observed using GSP which means that Cr (VI) is adsorbed over iron present on the GSP-Fe pellets. The adsorption energy values agree with this observation, as the adsorption energy of Cr (VI) is much lower than that of iron and does not favour the displacement of Fe(III) ions.

3.3.3. Cr(VI) elimination by GSP-Fe(0)

Further studies were carried out to study the elimination process of chromium by GSP-Fe(0). As we mentioned before, the purpose of the process is to eliminate as much Cr(VI) as possible. pH studies showed that the maximum Cr(VI) elimination is achieved under acidic conditions (pH = 1) (Fig. 9). As it can be seen in Fig. 9, Cr(VI) elimination decreases significantly with the increase of the pH, disappearing when the pH is higher than 5.

GSP-Fe(0) suffers a colour reversal from black to the characteristic red of the GSP-Fe during the removal process. This colour change implies the reversal of the process performed by the eucalyptus extract, re-oxidizing Fe(0) to Fe(III). The oxidation implies a reduction process of the $K_2Cr_2O_7$ acidic solution. This fact was confirmed during the experiments where Cr(VI) and total chromium measurements were done by UV–VIS and FAAS spectroscopy respectively. More total chromium than Cr(VI) was found in the reaction medium. This means that a fraction of the initial Cr(VI) was reduced to Cr(III), which agrees with the colour

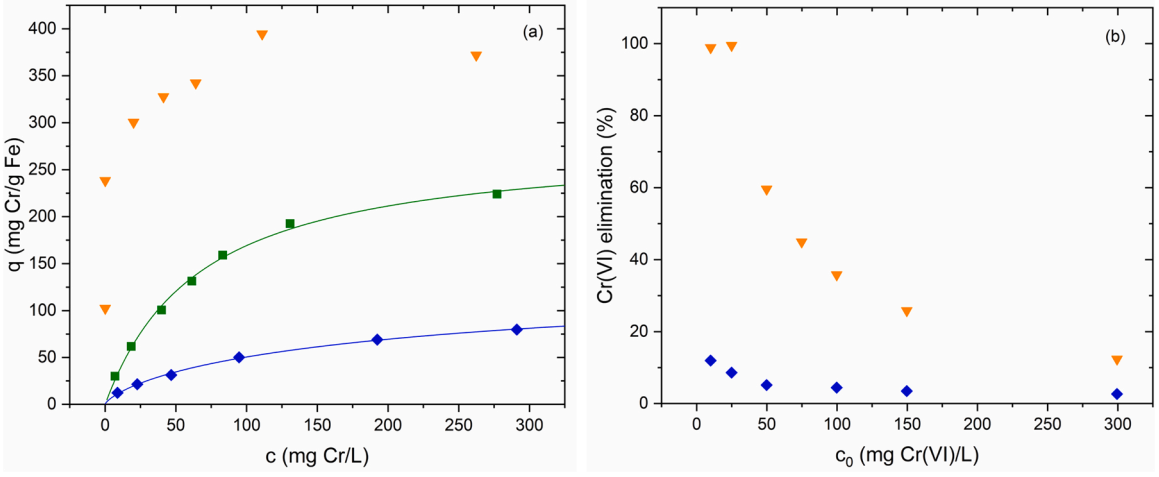

Fig. 8. (a) Equilibrium experimental data. (♦) Cr(VI) adsorption by GSP-Fe. (▼) Cr(VI) maximum elimination by GSP-Fe(0). (■) Total chromium adsorption by GSP-Fe(0). Solid lines were obtained by fitting to Eq. 2.(b) (♦) Cr(VI) elimination percentages by GSP-Fe. (▼) Cr(VI) elimination percentages by GSP-Fe(0). GSP-Fe/Fe(0) dose 4 $g{\cdot}L^{-1}$ equals to 98 $mg{\cdot}L^{-1}$ of Fe, pH 1, room temperature and agitation at 175 RPM for all the experiments. Initial Cr(VI) concentration from 10 to 300 $mg{\cdot}L^{-1}$.

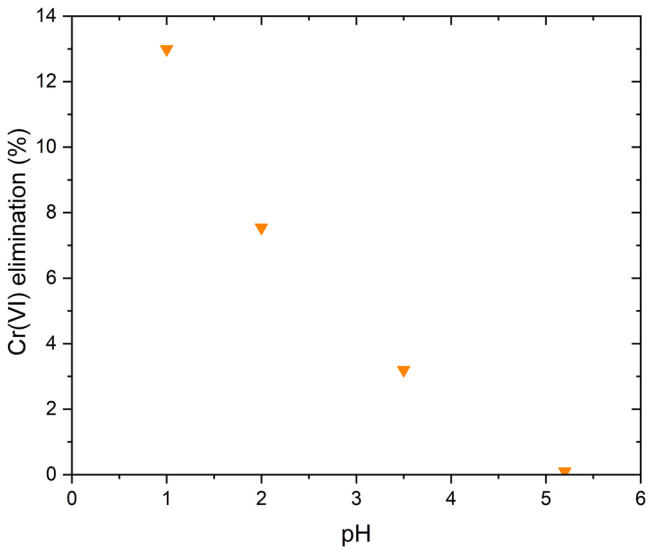

Fig. 9. Effect of pH on Cr(VI) elimination by GSP-Fe(0). GSP-Fe(0) dose 2 g·L^{-1}. Initial Cr(VI) concentration 100 mg·L^{-1}, room temperature and agitation at 175 RPM.

change observed in the GSP-Fe(0) pellets. The following reaction is proposed.

$$Cr_2O_7^{2-} + 2Fe + 14H^+ \rightleftarrows 2Cr^{3+} + 2Fe^{3+} + 7H_2O \quad (4)$$

As it is indicated in Section 3.1, Cr(VI) sorption was observed on GSP-Fe pellets, so the full chromium elimination process when GSP-Fe(0) is used consists of a combined reduction-adsorption process. First, a reduction process of the Cr(VI) to Cr(III) where the Fe(0) contained in the GSP-Fe(0) is oxidised to Fe(III). Second, a fraction of the Cr(VI) remaining in the solution is absorbed by the Fe(III) generated by the oxidation. This agrees with the results from EDS images in Fig. 4, which shows that chromium is preferentially adsorbed in the Fe-dominated zone.

Kinetic studies showed that equilibrium is reached in approximately 20 h. Colour change occurs during the first hour and most of the reaction takes place in 7 h. Kinetic reaction was fitted to the pseudo-second order model. Pseudo-second order parameters are shown in Table 2 and the kinetics plot can be found in the Supplementary material.

The chromium elimination process is not a pure adsorption reaction, so equilibrium studies between GSP-Fe(0) and Cr(VI) were divided into several stages: Cr(VI) elimination by the reduction-adsorption process, total chromium adsorption capacity and Cr(III) adsorption. In the case of Cr(VI) elimination, the data from the equilibrium studies cannot be fitted to a pure adsorption model; consequently, percentage removal rates and elimination capacities without further fitting were calculated.

As Fig. 8b shows, 0.2 g of GSP-Fe(0) containing approximately 4.9 mg iron achieves 100 % removal of Cr(VI) in 50 ml solution up to 25 mg·L^{-1} which is far superior to the elimination of Cr(VI) by GSP-Fe. In Fig. 8a, it can be seen that the amount of Cr(VI) removed per g of Fe (q) increases with the concentration of Cr(VI) in solution with an isotherm trend, reaching a plateau, indicating that the material reaches saturation. From this plateau, the maximum Cr(VI) elimination that GSP-Fe(0) achieved by the combined adsorption-reduction process is obtained (Table 3).

The maximum amount of Cr(VI) removed by reduction (230.21 mg·g^{-1}; 4.42 mmol·g^{-1}) can be calculated by subtracting the amount of Cr(VI) adsorbed (153 mg·g^{-1}; 2.94 mmol·g^{-1}) from the maximum amount of Cr(VI) removed (383.21 mg·g^{-1}; 7.37 mmol·g^{-1}). This quantity indicates a ratio of 0.5: 2 between Cr(VI) and Fe(0), although the stoichiometric ratio of the reduction reaction is 2: 2 (Eq. 4). Two hypotheses are suggested to explain the reason why the experimental ratio is lower than the stoichiometric ratio.

A secondary reaction of H^+ reduction by Fe(0) (Eq. 5) can occur due to the presence of a high concentration of H^+ in the reaction medium, as it is suggested in other studies [14,27].

$$Fe + 2H^+ \rightarrow Fe^{2+} + H_{2(g)} \quad (5)$$

This reaction is considered secondary in the Cr(VI) removal process because during the stability studies, GSP-Fe(0) pellets were submerged into an HCl solution at pH 1 for a long time until the disappearance of the characteristic black colour of GSP-Fe(0) and the appearance of the red colour of GSP-Fe. The time is longer (12–24 h) than Cr(VI) elimination process (approximately 60 min). Colour change does not happen when deionised water is used instead of the HCl solution. Fe(II) generated in this reaction can be rapidly oxidised to Fe(III) on the surface of the material as occurs during the adsorption process.

On the other hand, not all the Fe(III) adsorbed on the pellets might be accessible to the extract. In this situation, the treatment with the extract does not produce the maximum amount of Fe(0) possible regarding the Fe(III) present in the material, decreasing the amount of Cr(VI) removed by reduction.

3.3.4. Total chromium sorption by GSP-Fe(0)

Cr(VI) is mainly eliminated by a process that consists of a reduction of Cr(VI) to Cr(III), so during the equilibrium studies total chromium sorption was also analysed. Cr(VI) removed by reduction remains in the reaction medium as Cr(III). However, when total chromium (Cr(VI) and Cr(III) in solution) was analysed, it was found that the concentration at the equilibrium was lower than the initial Cr(VI) concentration. A fraction of the total chromium must therefore be retained in the material by adsorption. The adsorption model described in Eq. 2 was used to fit the data. Fig. 8a shows total chromium adsorption fitted using Eq. 2, and the fitting parameters obtained with the three isotherm models are summarised in Table 3. All models describe properly the experimental data. In this case, the error obtained for the parameter Q_o is higher than the one obtained in the equilibrium of the iron adsorption by GSP, but lower than in the Cr(VI) sorption process by GSP-Fe due to the fact that the saturation zone of the isotherm is not clearly defined, unlike in the process between Fe and GSP where a plateau is clearly seen (Fig. 6b). Although the saturation zone is not well defined, the end of the isotherm is very close to this zone, so the $c_{½}$ and b parameters have a much lower error than in the case of Cr(VI) adsorption.

Finally, the effects of temperature and ionic strength on the adsorption process was studied. Results showed that in the temperature range studied (10–52 °C) there were no differences in the adsorption values. At higher temperatures, degradation of the material was observed, so it is not feasible to study the effect at temperatures above 60 °C. In similar adsorption studies, we have also observed that there is no noticeable influence of temperature on the adsorption process [37–39]. There is also no significant difference in the values obtained for Cr(VI) removal and total chromium adsorption in the range studied (I from 0.05 M to 0.5 M). The value of I = 0.05 M corresponds to the ionic strength in the elimination process without adding electrolyte.

Further information can be found in the Supplementary material: Cr (VI) and total chromium sorption experimental data fitted using Langmuir and Langmuir-Freundlich models, temperature effect experimental data and the experimental data of the influence of the ionic strength.

3.3.5. Cr(III) sorption by GSP-Fe(0)

When the equilibrium between GSP-Fe(0) and Cr(III) at pH 1 was studied, it was observed that there was no adsorption of Cr(III) on the material. However, due to the difference observed in the Fig. 8a between the adsorption of total Cr by GSP-Fe(0) and the adsorption of Cr(VI) by GSP-Fe, an experiment was designed to check if the presence of Cr(VI) adsorbed on the pellets could favour the adsorption of Cr(III). Results confirmed the presence of Cr(III) adsorbed on the pellets that had

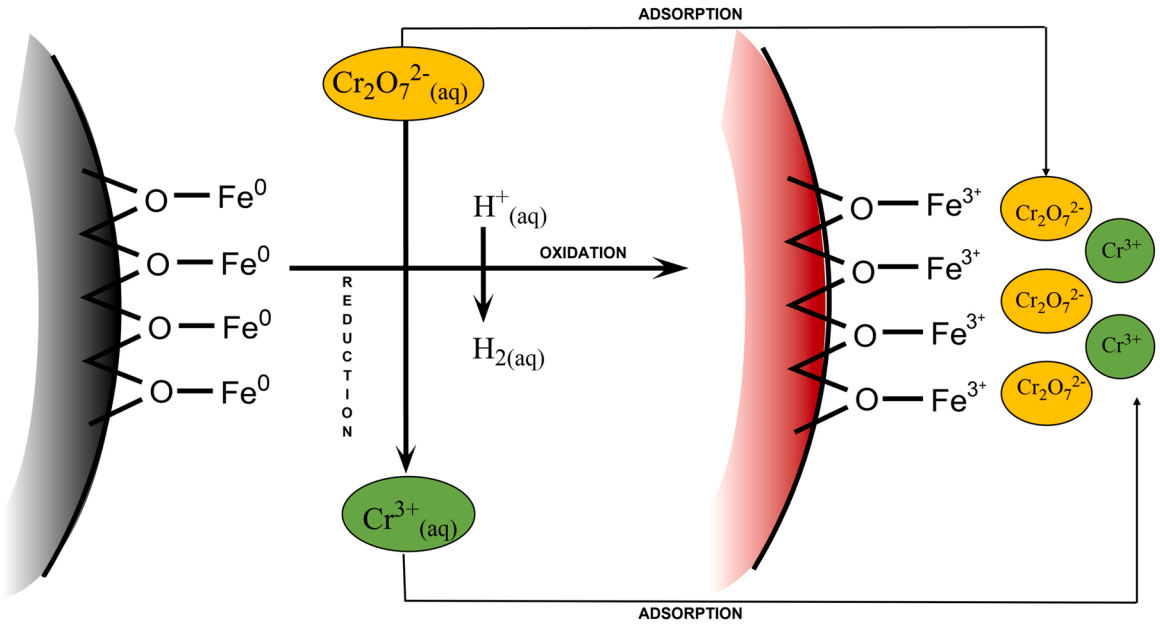

Fig. 10. Schematic diagram of the Cr(VI) elimination process performed by GSP-Fe(0).

previously adsorbed Cr(VI), indicating that Cr(III) is adsorbed in the areas where Cr(VI) is present. Fig. 10 shows the proposed scheme for the chromium elimination process.

3.3.6. *GSP-Fe(0) service life*

A test was carried out with GSP-Fe(0) to check how many times it can be used efficiently to eliminate chromium by regenerating the Fe(0) with eucalyptus extract (Fig. 11). The process was the same as in the equilibrium studies. 0.2 g of GSP-Fe(0) were immersed in Cr(VI) solutions at pH 1 for 24 h. When equilibrium was reached, the chromium solution was removed, and the material was treated again with eucalyptus extract to regenerate the Fe(0). After the treatment, the material was immersed in a new Cr(VI) solution with the same initial concentration as the previous one. In the first elimination, GSP-Fe(0) results were similar to those obtained in the equilibrium studies. In the second elimination, Cr(VI) removal efficiency decreased by 27.5 %, while the adsorption of total Cr was maintained. After this cycle, a SEM analysis was done (Fig. 1d). In the third elimination, Cr(VI) removal decreased by 59 % compared to the first elimination, and total chromium adsorption decreased by 15 %. The efficiency of the reduction step is affected by the increased presence of Cr(VI) in the material throughout the cycles. Cr(VI) may decrease the efficiency when treating the material with eucalyptus extract to regenerate Fe(0), as it is a strong oxidant. In the case of chromium adsorption, the performance starts to decrease when the material is saturated.

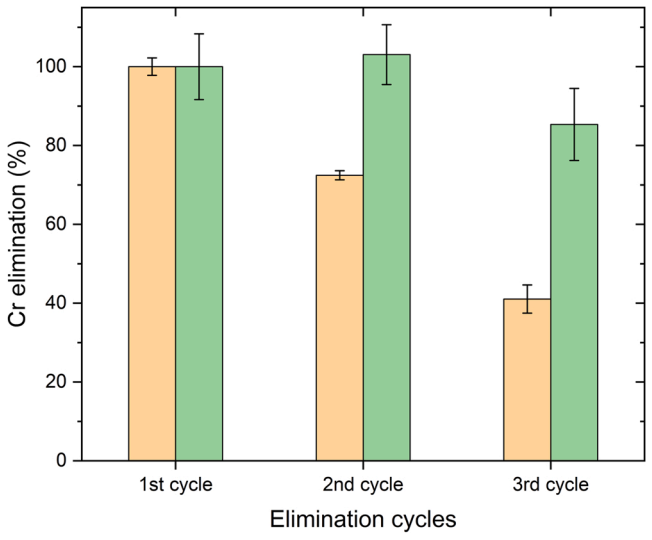

Fig. 11. Material service life. Left bar (orange), elimination percentages of Cr (VI) for each elimination cycle. Right bar (green), elimination percentages of total chromium for each elimination cycle. GSP-Fe(0) dose 4 g·L^{-1}, pH 1, room temperature and agitation at 175 RPM. Initial Cr(VI) concentration 50 mg·L^{-1}.

3.3.7. *Material stability after the elimination cycles*

Different tests were done to check the stability of the materials after the elimination cycles. No mechanical degradation or iron release into the solution was observed. The GSP-Fe(0) pellets were weighed before and after the elimination cycles. 0.1239 g of GSP-Fe(0) weighed 0.1218 g after the cycles, hence a negligible weight loss was observed. GSP-Fe(0) diameter and thickness were also checked. An average diameter of 3 mm was measure both before and after sorption cycle. The thickness of the pellets also remains constant, being 1 mm. After the three cycles, a BET surface area of 402.7 $m^2 \bullet g^{-1}$ and a pore volume of 0.50 $cm^3 \bullet g^{-1}$ were found. These values are slightly lower than the ones found for the plain GSP-Fe(0) (481.8 $m^2 \bullet g^{-1}$ and 0.55 $cm^3 \bullet g^{-1}$), which is attributable to the decrease in the surface area due to chromium adsorption. In conclusion a good mechanical stability of the material was observed after three sorption cycles.

3.3.8. *Material performance*

Table 4 shows the good results obtained for the removal of Cr(VI) and total chromium. GSP-Fe(0) surpasses other low-cost materials [40–43] and materials used in industry for Cr(VI) treatment such as $NaHSO_3$ without generating sludge as by-products of the process [44]. Results are good even after three elimination cycles (157.12 mg·g^{-1}, 3.02 mmol·g^{-1}). This material has another important advantage among other substances used to remove chromium. It can reduce chromate to Cr(III) and adsorb both species without the need for modifications to the reaction medium (e.g. changing the pH or adding a reagent) between the reduction and adsorption processes [27]. GSP-Fe(0) is stable in the reaction medium and is easily removed from it when reaction has finished by decantation or filtration. The main limitation of the material is the amount of iron that it can adsorb. Increasing the ratio of iron per mass of

Table 4
Cr(VI) and total chromium removal values obtained in this study, compared with other values found in bibliography. The Cr(VI) elimination column indicates the maximum amount of Cr(VI) that the materials can eliminate, mainly by reduction to Cr(III). The total chromium adsorption column indicates the amount of chromium (VI and III) that the materials can remove from solution by adsorption.

Cr (VI) elimination			Total chromium sorption		
Quantity ($mg \cdot g^{-1}$)	Material	Reference	Quantity ($mg \cdot g^{-1}$)	Material	Reference
383.2	GSP-Fe(0)	This study	279.40	GSP-Fe(0)	This study
408.2	SO_2	[44]	315.16	Activated carbon (CKW)	[41]
333.8	$NaHSO_3$	[44]	154	Chitosan	[40]
252.7	Bracken fern	[42,43]	83	Bracken fern	[42,43]
118.6	*Sargassum muticum*	[11,42]	18	*Sargassum muticum*	[11,42]
0.7	Fe(0) assisted by silica	[27]	1.36	Fe(0) assisted by silica	[27]

silica gel as much as possible will grant high chromium removals with small amounts of Supporting material. This can be achieved by reducing the pellet size to increase the surface exposed, although it could affect the stability of the pellet. To avoid problems that may arise, such as breakage of the material at the time of hydration, an improvement of the pellet stability may be required by increasing its mechanical strength, so that it remains stable in the reaction medium.

4. Conclusions

Fe(0) dopped silica material provides good results as a Cr(VI) remover (383.21 mg $Cr \cdot g^{-1}$ Fe(0)). GSP is cheap and easy to produce, and it has a high affinity for iron, with a high adsorption energy.

The functionalised material (GSP-Fe(0)) is stable in the reaction media due to the organic matter acting as a capping agent. This organic layer is retained in the material during the treatment with eucalyptus extract, which means that the green synthesis approach is key in the preparation of a stable material. GSP-Fe(0) can be used for several elimination cycles with good results (from 383.21 mg $Cr(VI) \cdot g^{-1}$ Fe(0) in the first cycle down to 157.12 $mg \cdot g^{-1}$ in the third one).

The most relevant feature of GSP-Fe(0) is its ability to achieve high Cr(VI) eliminations by a combined reduction-adsorption process in a single step, without the need to vary the conditions of the medium. Besides this reaction does not produce by-products such as sludge, which are produced by other chemical decontamination methods. In addition, it is easily removable from the medium after the process by filtration or decantation, which is the main problem associated to the use of nanoparticles as adsorbents.

Fe(0) is the active species that works as Cr(VI) remover while GSP only acts as a Supporting material. Owing to this reason, it is interesting to increase the maximum amount of Fe adsorbed on the GSP pellets to achieve high Cr(VI) removal rates using as less material as possible. This can be achieved by reducing the pellet size, which would increase the adsorption surface area.

GSP-Fe(0) is simple to produce, inexpensive and easy to handle. These properties are a major advantage over other materials that are much more complex or expensive to produce, and which achieve a similar performance.

These advantages make GSP-Fe(0) a good candidate to be studied as a packing in adsorption columns.

CRediT authorship contribution statement

David Gómez-Carnota: Investigation, Writing original-draft, Writing review & editing, Formal analysis. José L. Barriada: Writing review & editing, Supervision, Conceptualization, Funding acquisition, Data curation. Roberto Herrero: Writing review & editing, Supervision, Conceptualization, Funding acquisition, Project administration.

Declaration of Competing Interest

The authors declare that they have no known competing financial interests or personal relationships that could have appeared to influence the work reported in this paper.

Data availability

Data will be made available on request.

Acknowledgments

Authors wish to thank Agencia Estatal de Investigación (AEI) (Ministerios de Ciencia e Innovación y de Economía y Competitividad) for the financial support through the research projects PID2020–117910 GB-C22 and CTQ2016–80473-P cofounded with FEDER (UE) programme. Gómez-Carnota thanks Fundación Segundo Gil Dávila for the fellowship grant.

Appendix A. Supporting information

Supplementary data associated with this article can be found in the online version at doi:10.1016/j.jece.2022.108258.

References

[1] Agency for Toxic Substances and Disease Registry, ATSDR's Substance Priority List, https://www.atsdr.cdc.gov/SPL/#2019spl, 2019, (accessed on 26 April 2021).
[2] United States Environmental Protection Agency, Urban Air Toxic Pollutants, https://www.epa.gov/urban-air-toxics/urban-air-toxic-pollutants, (accessed on 26 April 2021),
[3] United States Environmental Protection Agency, Initial List of Hazardous Air Pollutants with Modifications, https://www.epa.gov/haps/initial-list-hazardous-air-pollutants-modifications#mods, (accessed on 26 April 2021),
[4] F.C. Richard, A.C.M. Bourg, Aqueous geochemistry of chromium: a review, Water Res. 25 (1991) 807–816, https://doi.org/10.1016/0043-1354(91)90160-R.
[5] S. Mishra, R.N. Bharagava, Toxic and genotoxic effects of hexavalent chromium in environment and its bioremediation strategies, J. Environ. Sci. Health Pt. C. -Environ. Carcinog. Ecotoxicol. Rev. 34 (2016) 1–32, https://doi.org/10.1080/10590501.2015.1096883.
[6] P. Miretzky, A.F. Cirelli, Cr(VI) and Cr(III) removal from aqueous solution by raw and modified lignocellulosic materials: a review, J. Hazard. Mater. 180 (2010) 1–19, https://doi.org/10.1016/j.jhazmat.2010.04.060.
[7] M. Shahid, S. Shamshad, M. Rafiq, S. Khalid, I. Bibi, N.K. Niazi, C. Dumat, M. I. Rashid, Chromium speciation, bioavailability, uptake, toxicity and detoxification in soil-plant system: a review, Chemosphere 178 (2017) 513–533, https://doi.org/10.1016/j.chemosphere.2017.03.074.
[8] A. Kumar, H.M. Jena, Adsorption of Cr(VI) from aqueous solution by prepared high surface area activated carbon from Fox nutshell by chemical activation with H3PO4, J. Environ. Chem. Eng. 5 (2017) 2032–2041, https://doi.org/10.1016/j.jece.2017.03.035.
[9] U.O. Aigbe, O.A. Osibote, A review of hexavalent chromium removal from aqueous solutions by sorption technique using nanomaterials, J. Environ. Chem. Eng. 8 (2020), 104503, https://doi.org/10.1016/j.jece.2020.104503.
[10] P. Lodeiro, Á. Gudiña, L. Herrero, R. Herrero, M.E. Sastre de Vicente, Aluminium removal from wastewater by refused beach cast seaweed. Equilibrium and dynamic studies, J. Hazard. Mater. 178 (2010) 861–866, https://doi.org/10.1016/j.jhazmat.2010.02.017.
[11] M. Lopez-Garcia, P. Lodeiro, R. Herrero, M.E. Sastre de Vicente, Cr(VI) removal from synthetic and real wastewaters: the use of the invasive biomass Sargassum muticum in batch and column experiments, J. Ind. Eng. Chem. 18 (2012) 1370–1376, https://doi.org/10.1016/j.jiec.2012.01.036.
[12] E. Romera, F. González, A. Ballester, M.L. Blázquez, J.A. Muñoz, Comparative study of biosorption of heavy metals using different types of algae, Bioresour. Technol. 98 (2007) 3344–3353, https://doi.org/10.1016/j.biortech.2006.09.026.
[13] P.K. Tandon, R.C. Shukla, S.B. Singh, Removal of Arsenic(III) from water with clay-supported zerovalent iron nanoparticles synthesized with the help of tea liquor, Ind. Eng. Chem. Res. 52 (2013) 10052–10058, https://doi.org/10.1021/ie400702k.
[14] J. Yang, S. Wang, N. Xu, Z. Ye, H. Yang, X. Huangfu, Synthesis of montmorillonite-supported nano-zero-valent iron via green tea extract: enhanced transport and

application for hexavalent chromium removal from water and soil, J. Hazard. Mater. 419 (2021), 126461, https://doi.org/10.1016/j.jhazmat.2021.126461.
[15] M. Martinez-Cabanas, M. Lopez-Garcia, J.L. Barriada, R. Herrero, M.E. Sastre de Vicente, Green synthesis of iron oxide nanoparticles. Development of magnetic hybrid materials for efficient As(V) removal, Chem. Eng. J. 301 (2016) 83–91, https://doi.org/10.1016/j.cej.2016.04.149.
[16] A. Sabín López, M. Paredes Ramos, R. Herrero, J.M.L.ópez Vilariño, Synthesis of magnetic green nanoparticle – molecular imprinted polymers with emerging contaminants templates, J. Environ. Chem. Eng. 8 (2020), 103889, https://doi.org/10.1016/j.jece.2020.103889.
[17] S.C.N. Tang, I.M.C. Lo, Magnetic nanoparticles: essential factors for sustainable environmental applications, Water Res. 47 (2013) 2613–2632, https://doi.org/10.1016/j.watres.2013.02.039.
[18] M. Martinez-Cabanas, L. Carro, M. Lopez-Garcia, R. Herrero, J.L. Barriada, M. E. Sastre de Vicente, Achieving sub-10 ppb arsenic levels with iron based biomass-silica gel composites, Chem. Eng. J. 279 (2015) 1–8, https://doi.org/10.1016/j.cej.2015.04.148.
[19] N. Ezzatahmadi, G.A. Ayoko, G.J. Millar, R. Speight, C. Yan, J. Li, S. Li, J. Zhu, Y. Xi, Clay-supported nanoscale zero-valent iron composite materials for the remediation of contaminated aqueous solutions: a review, Chem. Eng. J. 312 (2017) 336–350, https://doi.org/10.1016/j.cej.2016.11.154.
[20] E.W. Rice, R.B. Baird, A.D. Eaton, L.D. Clesceri. Standard Methods For the Examination of Water and Wastewater, American Public Health Association, Washington DC, 2012, pp. 365–368.
[21] E.W. Rice, R.B. Baird, A.D. Eaton, L.D. Clesceri. Standard Methods For the Examination of Water and Wastewater, American Public Health Association, Washington DC, 2012, pp. 358–360.
[22] S. Brunauer, L.S. Deming, W.E. Deming, E. Teller, On a theory of the van der Waals adsorption of gases, J. Am. Chem. Soc. 62 (1940) 1723–1732, https://doi.org/10.1021/ja01864a025.
[23] M. Naderi, Chapter fourteen - Surface area: Brunauer–Emmett–Teller (BET), in: S. Tarleton (Ed.), Progress in Filtration and Separation, Academic Press, Oxford, 2015, pp. 585–608.
[24] S. Azizian, Kinetic models of sorption. A theoretical analysis, J. Colloid Interface Sci. 276 (2004) 47–52, https://doi.org/10.1016/j.jcis.2004.03.048.
[25] B. Beverskog, I. Puigdomenech, Revised pourbaix diagrams for iron at 25–300 °C, Corros. Sci. 38 (1996) 2121–2135, https://doi.org/10.1016/S0010-938X(96)00067-4.
[26] L. Sellaoui, H. Guedidi, S. Knani, L. Reinert, L. Duclaux, A. Ben Lamine, Application of statistical physics formalism to the modeling of adsorption isotherms of ibuprofen on activated carbon, Fluid Phase Equilib. 387 (2015) 103–110, https://doi.org/10.1016/j.fluid.2014.12.018.
[27] Y.J. Oh, H. Song, W.S. Shin, S.J. Choi, Y.-H. Kim, Effect of amorphous silica and silica sand on removal of chromium(VI) by zero-valent iron, Chemosphere 66 (2007) 858–865, https://doi.org/10.1016/j.chemosphere.2006.06.034.
[28] Z. Li, L. Sellaoui, G.L. Dotto, A. Bonilla-Petriciolet, A. Ben Lamine, Understanding the adsorption mechanism of phenol and 2-nitrophenol on a biopolymer-based biochar in single and binary systems via advanced modeling analysis, Chem. Eng. J. 371 (2019) 1–6, https://doi.org/10.1016/j.cej.2019.04.035.
[29] Z. Li, L. Sellaoui, S. Gueddida, G.L. Dotto, A. Ben Lamine, A. Bonilla-Petriciolet, M. Badawi, Adsorption of methylene blue on silica nanoparticles: Modelling analysis of the adsorption mechanism via a double layer model, J. Mol. Liq. 319 (2020), 114348, https://doi.org/10.1016/j.molliq.2020.114348.
[30] I.N. Levine, Physical chemistry. McGraw-Hill Companies, fifth ed., INC. USA, New York, 2002.
[31] M.M. Jiménez-Carmona, M.D. Luque de Castro, Isolation of eucalyptus essential oil for GC-MS analysis by extraction with subcritical water, Chromatographia 50 (1999) 578–582, https://doi.org/10.1007/BF02493664.
[32] S.S. Cheng, C.G. Huang, Y.J. Chen, J.J. Yu, W.J. Chen, S.T. Chang, Chemical compositions and larvicidal activities of leaf essential oils from two eucalyptus species, Bioresour. Technol. 100 (2009) 452–456, https://doi.org/10.1016/j.biortech.2008.02.038.
[33] M. Martínez-Cabanas, M. López-García, P. Rodríguez-Barro, T. Vilariño, P. Lodeiro, R. Herrero, J.L. Barriada, M.E. Sastre de Vicente, Antioxidant capacity assessment of plant extracts for green synthesis of nanoparticles, Nanomaterials 11 (2021) 1679, https://doi.org/10.3390/nano11071679.
[34] I. Alghoraibi, C. Soukkarieh, R. Zein, A. Alahmad, J.G. Walter, M. Daghestani, Aqueous extract of Eucalyptus camaldulensis leaves as reducing and capping agent in biosynthesis of silver nanoparticles, Inorg. Nano-Met. Chem. 50 (2020) 895–902, https://doi.org/10.1080/24701556.2020.1728315.
[35] B. Schrader, Infrared and Raman Spectroscopy. Methods and applications. VCH Verlagsgesellschaft mbH, First ed., Weinheim, Germany, 1995.
[36] B.H. Stuart, Infrared Spectroscopy: Fundamentals and Applications. Chichester, West Sussex, First ed..,, John Wiley & Sons, Ltd,, England, 2004.
[37] M.E. Sastre de Vicente, R. Herrero, P. Lodeiro, B. Cordero, Biosorption of cadmium by Fucus spiralis, Environ. Chem. 1 (2004) 180–187, https://doi.org/10.1071/EN04039.
[38] P. Lodeiro, J.L. Barriada, R. Herrero, M.E. Sastre de Vicente, The marine macroalga Cystoseira baccata as biosorbent for cadmium(II) and lead(II) removal: kinetic and equilibrium studies, Environ. Pollut. 142 (2006) 264–273, https://doi.org/10.1016/j.envpol.2005.10.001.
[39] J.L. Barriada, R. Herrero, D. Prada-Rodríguez, M.E. Sastre de Vicente, Waste spider crab shell and derived chitin as low-cost materials for cadmium and lead removal, J. Chem. Technol. Biotechnol. 82 (2007) 39–46, https://doi.org/10.1002/jctb.1633.
[40] V.M. Boddu, K. Abburi, J.L. Talbott, E.D. Smith, Removal of hexavalent chromium from wastewater using a new composite chitosan biosorbent, Environ. Sci. Technol. 37 (2003) 4449–4456, https://doi.org/10.1021/es021013a.
[41] L. Khezami, R. Capart, Removal of chromium(VI) from aqueous solution by activated carbons: Kinetic and equilibrium studies, J. Hazard. Mater. 123 (2005) 223–231, https://doi.org/10.1016/j.jhazmat.2005.04.012.
[42] M. Lopez-Garcia, Estudio fisicoquímico del proceso de reducción-adsorción de Cr (VI) en medio acuoso sobre biomateriales de bajo coste, Dr. Thesis Univ. da Coruña (2013).
[43] M. Lopez-Garcia, P. Lodeiro, J.L. Barriada, R. Herrero, M.E. Sastre de Vicente, Reduction of Cr(VI) levels in solution using bracken fern biomass: batch and column studies, Chem. Eng. J. 165 (2010) 517–523, https://doi.org/10.1016/j.cej.2010.09.058.
[44] L.D. Benefield, J.F. Judkins, Jr., B.L. Weand (Eds.), Process Chemistry for Water and Wastewater Treatment, Prentice-Hall, Inc, Englewood Cliffs, N.J, 1982.